Origin of coherent G-band phonon spectra in single-wall carbon nanotubes

A. R. T. Nugraha, E. H. Hasdeo, G. D. Sanders, C. J. Stanton, and R. Saito

Origin of coherent G band phonon spectra in single wall carbon nanotubes

A. R. T. Nugraha[1], E. H. Hasdeo[1], G. D. Sanders[2], C. J. Stanton[2], R. Saito[1]

[1]*Department of Physics, Tohoku University, Sendai 980-8578, Japan*

[2]*Department of Physics, University of Florida,*

Box 118440, Gainesville, Florida 32611-8440, USA

(Dated: November 26, 2014)

Abstract

Coherent phonons in single wall carbon nanotubes (SWNTs) are observed as oscillations of the differential absorption coefficient as a function of time by means of pump-probe spectroscopy. For the radial breathing mode (RBM) of a SWNT, the coherent phonon signal is understood to be a result of the modulated diameter-dependent energy gaps due to the coherent RBM phonon oscillations. However, this mechanism might not be the dominant contribution to other phonon modes in the SWNT. In particular, for the G band phonons, which correspond to bond-stretching motions, we find that the modulation of the interatomic optical dipole (electron-photon) matrix element gives rise to a strong coherent G band phonon intensity comparable to the coherent RBM phonon intensity. We also further discuss the dependence of coherent G band and RBM phonon amplitudes on the laser excitation pulse width.

PACS numbers: 78.67.Ch,78.47.J-,73.22.-f,63.22.Gh,63.20.kd

I. INTRODUCTION

Single wall carbon nanotubes (SWNTs), characterized by the chiral index (n, m),[1] have been important materials that provide us with a one-dimensional model system to study the dynamics and interactions between electrons, photons, and phonons.[2] In particular, rapid advances in ultrafast pump-probe spectroscopy have allowed researchers to observe lattice oscillations of SWNTs with the same phase in real time, known as coherent phonon spectroscopy.[3–7] The coherent phonon motions can be observed as oscillations of optical properties, such as the differential transmittance $(\Delta T/T)$ or differential reflectivity $(\Delta R/R)$ as a function of delay time between pump and probe pulses. To excite a coherent phonon of a given frequency, it is necessary for the pump pulse to have a Fourier component at the phonon frequency. By performing a Fourier transform of the oscillations of $\Delta T/T$ or $\Delta R/R$ with respect to time, we can obtain the coherent phonon spectra as a function of phonon frequency. Several peaks found in the coherent phonon spectra of a SWNT correspond to Raman active phonon modes, such as the radial breathing modes (RBMs), D bands, G bands, and G' bands.[8] Lim *et al.* showed that even the low-frequency acoustic phonon signals can be observed in purified $(6, 5)$ SWNTs by coherent phonon spectroscopy because of its ultrafine spectral resolution.[9] Moreover, ultrafast spectroscopy techniques allow us to directly measure phonon dynamics, including phase information, or life time of phonons, in the time domain.[3,4,6]

It is known that oscillations of $\Delta T/T$ or $\Delta R/R$ as a function of delay time t between pump and probe pulses in coherent phonon spectroscopy are directly related to the modulations of the absorption coefficient α as a function of the probe energy E_{probe} and t.[10] Therefore, in order to obtain the coherent phonon spectra theoretically, we need to calculate the absorption coefficient $\alpha(E_{\text{probe}}, t)$ for a given coherent phonon amplitude. In the case of RBMs, the oscillations of $\alpha(E_{\text{probe}}, t)$ have been understood as a result of energy gap modulations, which are inversely proportional to the nanotube diameter.[4,6] However, in the case of G bands, which are assigned to longitudinal-optical (LO) and in-plane transverse-optical (iTO) phonon modes,[2] it is known that these modes do not significantly modify the energy gaps because the SWNT diameters are not sensitive to the LO/iTO vibrations. While the coherent G band signals are experimentally observed to be on the same order of magnitude as the RBM signals,[9,11] our previous theoretical calculation predicted that the modulations

of absorption coefficient due to the G band (LO) phonons are about 1000 times smaller than those caused by the RBM.[12] We expect that the reason for the discrepancy is because we considered only the change of the energy gap as a main contribution for the coherent G band spectra and also because the excitation pulse used in the calculation was too long (50 fs) compared to the G band oscillation period (20 fs). This fact indicates that a different mechanism is necessary to explain the coherent G band intensity and that the effects of laser pulse width on the coherent phonon intensity should be taken into account, both of which are the main subjects of this paper.

One possible dominant contribution to the coherent G band intensity is the modulation of electron-photon interaction. For example, Grüneis *et al.* discussed the optical absorption of graphene from π to π^* bands, where the interatomic optical dipole matrix elements for the nearest neighbor carbon-carbon atoms, m_{opt}, are essential.[13] The optical matrix elements are thus sensitive to the change in the carbon-carbon bond length, which can be significantly modified by the G band phonons. In this work, in addition to the changes in electronic structure which arise from the coherent phonons, we now consider changes to the optical matrix element which arise from the coherent phonon oscillations. We find that modulation of m_{opt} is particularly relevant to the coherent G band intensity and that the changes to the optical matrix element for the G band are larger than for the RBM oscillations. We calculate the coherent G band spectra for a specified SWNT chirality and compare them with the other coherent phonon modes in the SWNT. By a simple analytical model, we also study how the variation of the laser pulse width affects the coherent phonon intensity.

This paper is organized as follows. In Section II, we explain coherent phonon simulation methods which include a general theory for the generation and detection of coherent phonons in SWNTs. In Section III, we present the main results and discuss how the coherent G band intensity could have a stronger signal by considering the modulation of optical interaction and shorter pulse width. And finally, we give a conclusion in Section IV.

II.   SIMULATION METHODS

To calculate coherent phonon spectra, we follow the methods described in our earlier papers,[12,14] except that we will also now treat the effects of the coherent phonon modulations of the electron-photon interaction which we previously neglected for simplicity. We define a

coherent phonon mode with wavevector $q = 0$ (Γ point phonon) whose amplitude satisfies a driven oscillator equation

$$\frac{\partial^2 Q_m(t)}{\partial t^2} + \omega_m^2 Q_m(t) = S_m(t), \tag{1}$$

where m and ω_m denote the phonon mode (e.g. RBM, oTO, LO, iTO) and its frequency, respectively. Equation (1) is solved subject to the initial conditions $Q_m(0) = 0$ and $\dot{Q}_m(0) = 0$. The driving function $S_m(t)$ in the right hand side of Eq. (1) is given by

$$S_m(t) = -\frac{2\omega_m}{\hbar} \sum_{nk} \mathcal{M}_n^m(k) \left(f_n(k, t) - f_n^0(k) \right). \tag{2}$$

where $f_n(k, t)$ is the time-dependent electron distribution function and $f_n^0(k)$ is the initial equilibrium electron distribution function. Here n labels an electronic state, while k gives the electron wavevector. The electronic states of a SWNT are calculated within the extended tight-binding (ETB) approximation.[15] The electron-phonon matrix element $\mathcal{M}_n^m(k)$ in Eq. 2 is a shorthand for $\mathcal{M}_{nk;nk}^{m,0}$, where $\mathcal{M}_{n'k';nk}^{m,q}$ is the deformation potential electron-phonon matrix element in the ETB model with phonon wavevector $q = k - k'$ and with a transition from the state n to n'.[16]

From Eq. (2), we see that the driving function $S_m(t)$ depends on the photoexcited electron distribution functions, which can be calculated generally by taking photogeneration and relaxation effects into account. The electron-phonon matrix element in this equation tells us that the coherent phonon oscillations are basically generated by the time-dependent electronic population through the electron-phonon interaction, while the electronic population is induced by the optical pulse through the electron-photon interaction. Besides creating the electronic population, the ultrafast laser pulse also generates an interband polarization that oscillates much faster than the phonon modes considered in this study. It thus averages to zero and hence we neglect its contribution for simplicity. The observed coherent phonon intensity is then proportional to the power spectrum of the oscillations of optical properties.[10] Within the scope of this work, we ignore relaxation effects of the photoexcited carriers and consider only the rapidly varying photogeneration term which can be calculated directly from the Fermi's golden rule. Neglecting carrier relaxation has a negligible effect on the computed coherent phonon signal since the relaxation time is much greater than the laser pulse duration and the coherent phonon period.[12]

Using the Fermi's golden rule, we obtain the photogeneration rate for the distribution

functions as follows,[17]

$$\frac{\partial f_n(k)}{\partial t} = \frac{8\pi^2 e^2 \; u(t)}{\hbar \; n_g^2 \; (E_{\text{pump}})^2} \left(\frac{\hbar^2}{m_0}\right) \sum_{n'} |P_{nn'}(k,t)|^2$$
$$\times \left(f_{n'}(k,t) - f_n(k,t)\right) \delta\left(E_{nn'}(k,t) - E_{\text{pump}}\right), \tag{3}$$

where $E_{nn'}(k,t) = |E_n(k,t) - E_{n'}(k,t)|$ are the k dependent transition energies at time t of a coherent phonon oscillation, E_{pump} is the pump laser energy, $u(t)$ is the time-dependent energy density of the pump pulse, e is the electron charge, m_0 is the free electron mass, and n_g is the refractive index of the surrounding medium. The pump energy density $u(t)$ is related with the pump fluence F by a relation $F = (c/n_g) \int u(t)dt$ and $u(t)$ is also assumed to be a Gaussian. Thus

$$u(t) = A_p e^{-4t^2 \ln 2/2\tau_p^2}, \tag{4}$$

where $A_p = (2n_g F\sqrt{\ln 2/\pi})/(c\tau_p)$ and c is the speed of light. In Eq. (4), τ_p is defined as the pump duration or laser pulse width. Unless otherwise mentioned, we use parameters $\tau_p = 10\,\text{fs}$, $F = 10^{-5}$ J cm^{-2}, and $n_g = 1$. To also account for lifetime broadening of the photoexcited carriers during the absorption process, we replace the delta function in Eq. (3) with a Lorentzian lineshape

$$\delta(E_{nn'} - E_{\text{pump}}) \rightarrow \frac{\Gamma_p/(2\pi)}{(E_{nn'} - E_{\text{pump}})^2 + (\Gamma_p/2)^2}, \tag{5}$$

where $\Gamma_p = 0.15\,\text{eV}$ is the spectral linewidth (FWHM).[12] Here the time dependence of $E_{nn'}$ is determined by $Q_m(t)$ mainly through the RBMs, in which the energy dispersion is inversely proportional to the SWNT diameter.[4,12]

By considering light polarized parallel to the tube axis (z axis) that contributed to the optical absorption, we can write the optical matrix element $P_{nn'}$ in Eq. (3) within the dipole approximation as[13]

$$P_{nn'}(k) = \frac{\hbar}{\sqrt{2m_0}} \sum_{i,j\mathbf{J}} C_i^*(n',k)C_j(n,k)e^{i\phi_{\mathbf{J}}(k)}m_{\text{opt}}(i,j\mathbf{J}), \tag{6}$$

where $C_i(n,k)$ and $\phi_{\mathbf{J}}(k)$ respectively denote the expansion coefficient and phase factor from the Nth two-atom unit cell of the symmetry-adapted ETB wave functions.[18] The atomic electron-photon matrix element is given by

$$m_{\text{opt}} = \int d\mathbf{r}\varphi_{i0}^*(\mathbf{r} - \mathbf{R}_{i0})\frac{\partial}{\partial z}\varphi_{j\mathbf{J}}(\mathbf{r} - \mathbf{R}_{j\mathbf{J}}), \tag{7}$$

where $\varphi_{j\mathbf{J}}$ is the $2p_z$ orbital of the jth atom in the $\mathbf{J}$th unit cell.

We should note that Eqs. (6) and (7) still do not have an explicit time dependence. The time-dependence of the optical matrix element comes from the coherent phonon amplitude $Q_m(t)$ which allows the atomic matrix element m_{opt} to also vary as a function of time as the positions of the carbon atoms change. Grüneis $et.$ al calculated the integral in Eq. (7) for planar graphene analytically by expanding the orbital wavefunctions in terms of Gaussians and it was found that m_{opt} explicitly depends on the bond length between two carbon atoms a_{CC}.[13] If the bond length a_{CC} is altered by coherent phonon oscillations, the atomic matrix element m_{opt} is directly affected, as is the dipole optical (electron-photon) matrix element $P_{nn'}$. This is because the deformation of the bond lengths alters the transfer integral and overlap matrix elements in the ETB model.

Based on above argument, the time-dependence of $E_{nn'}(k,t)$ and $P_{nn'}(k,t)$ can be obtained from the time-dependent lattice displacements due to the change in a_{CC} by the coherent phonon oscillations, especially for the G band, which is the in-plane C-C bond-stretching mode. From the coherent phonon amplitudes, the time-dependent macroscopic displacement of each carbon atom in an SWNT is given by[12]

$$\mathbf{U}_{j\mathbf{J}}(t) = \frac{\hbar}{\sqrt{2M}} \sum_m \frac{\hat{\mathbf{e}}_{j\mathbf{J}}^m}{\sqrt{\hbar\omega_m}} Q_m(t) \tag{8}$$

where $\hat{\mathbf{e}}_{j\mathbf{J}}^m \equiv \hat{\mathbf{e}}_{j\mathbf{J}}^m(q = 0)$ is the unit phonon mode polarization for the jth atom in the $\mathbf{J} = (0,0)$ two-atom unit cell, $\hbar\omega_m \equiv \hbar\omega_m(q = 0)$, and M is the mass of a carbon atom. The bond length a_{CC} at each time t of a coherent phonon oscillation can then be calculated from the macroscopic carbon atom displacements. Eventually, the time-dependent optical matrix element can be evaluated by

$$P_{nn'}(k,t) = P_{nn'}(k,0) + \Delta P_{nn'}(k,t), \tag{9}$$

where $\Delta P_{nn'}(k,t)$ is directly proportional to the time-dependent m_{opt} and we take an average of $P_{nn'}$ over three nearest neighbor atoms.

In coherent phonon spectroscopy, a laser probe pulse is used to measure the time-varying absorption coefficient of the SWNT. The time-dependent absorption coefficient $\alpha(t)$ at a

probe energy E_{probe} is given by the Fermi's golden rule

$$\alpha(E_{\text{probe}}, t) \propto \sum_{nn'} \int dk \; |P_{nn'}(k,t)|^2 \Big(f_n(k,t) - f_{n'}(k,t) \Big)$$
$$\times \; \delta \Big(E_{nn'}(k,t) - E_{\text{probe}} \Big), \tag{10}$$

We replace the delta function in Eq. (10) with a broadened Lorentzian spectral lineshape with a FWHM of $\gamma = 0.15$ eV,[12] similar to that in Eq. (5). Excitation of coherent phonons by the laser pump modulates the optical properties of the SWNTs, which gives rise to a transient differential transmission signal, or the modulations of absorption coefficient. The time-resolved differential gain measured by the probe is then given by

$$\Delta\alpha(E_{\text{probe}}, t) = -[\alpha(\hbar\omega, t) - \alpha(\hbar\omega, t \to -\infty)] \tag{11}$$

We take the theoretical coherent phonon signal (or intensity, I) to be proportional to the Fourier power spectrum of such absorption modulations at a given energy E_{probe},

$$I(\omega) = \int e^{-i\omega t} \, |\Delta\alpha(E_{\text{probe}}, t)|^2 \, dt, \tag{12}$$

where ω represents the phonon frequency that contributes to the coherent phonon spectra.

III. RESULTS AND DISCUSSION

A. Modulation of optical interaction

First we discuss the effects of coherent phonon oscillations on the optical interaction. The changes in a_{CC} modulate the atomic matrix element m_{opt} because of the direct correspondence between these two quantities at time t. Fig. 1(a) shows the calculated m_{opt} as a function of a_{CC} based on the formula given by Grüneis et $al.$[13,19]. It indicates that the strength of optical interaction monotonically decreases as a function of a_{CC}. In the inset of Fig. 1(a), we show the atomic matrix element within an enlarged region around $1.40\,\text{Å}$ and $1.45\,\text{Å}$. The shaded region corresponds to the possible values of a_{CC} affected by the coherent LO phonon oscillation given in Fig. 1(b). From this figure, we can say that the modulations of optical interaction is about 0.02 [a.u]$^{-1}$ for the change of vibration amplitude of about $0.02\,\text{Å}$. These modulations of optical interaction is thus approximately $10\,\%$ of $m_{\text{opt}} = 0.25$[a.u.]$^{-1}$, which is not negligible for calculating the absorption coefficient of a
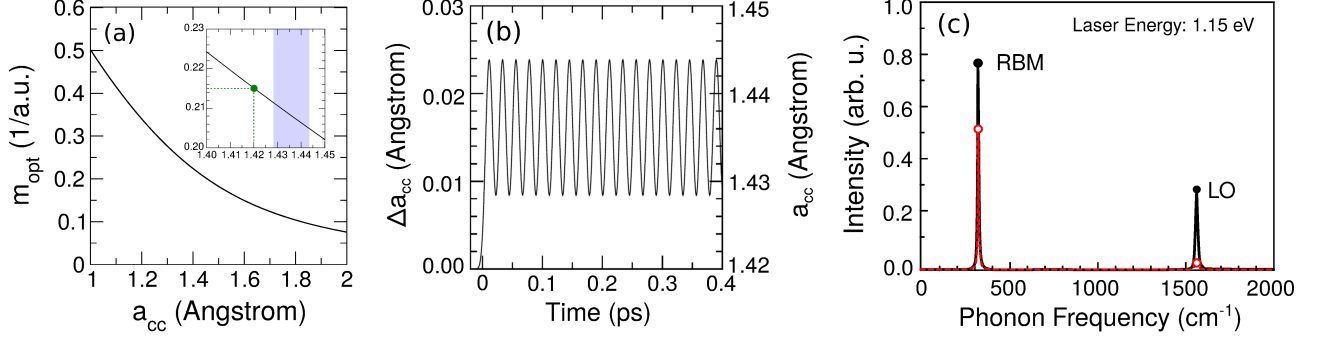
FIG. 1: (a) Atomic matrix element as a function of carbon-carbon bond length in SWNTs and (b) the change of bond length as a function of time due to a coherent LO phonon oscillation of in a $(6,5)$ SWNT at a laser (both pump and probe) energy of $1.15\,\mathrm{eV}$. Inset in (a) shows an enlarged region between $1.40\,\text{Å}$ and $1.45\,\text{Å}$. A dot in the inset corresponds to the bond length without coherent phonon oscillations, whereas the shaded region corresponds to the area in which the bond length oscillates as shown in (b). (c) Coherent phonon intensity as a function of phonon frequency, showing the RBM and LO peaks. Solid (dashed) line is the calculated result with (without) considering the modulation of optical matrix element. Filled (open) circles are also a guide for eyes to see the intensity values which include (exclude) the modulation of optical matrix element.

SWNT. The coherent phonon intensity is proportional to $|\Delta\alpha|^2 \propto |\Delta m_{\mathrm{opt}}|^4$, which is the leading order of the spectra. In the previous study, however, this fact was not taken into account and the optical matrix element was considered constant as a function of time.[12]

Next, from the time-dependent optical matrix elements, we proceed to the calculation of coherent phonon spectra by taking the Fourier transform of Eq. (11). The calculation is performed by allowing the probe energy in Eq. (10) to be varied independently while keeping the pump energy in Eq. (3) constant. We take a $(6,5)$ SWNT chirality as a sample for this calculation. This SWNT has the first and second optical transition energies (band gaps) of $1.27\,\mathrm{eV}$ and $2.42\,\mathrm{eV}$, denoted by E_{11} and E_{22}, respectively.[20] In this calculation we neglect the exciton effects for simplicity. Basically, the exciton-photon matrix elements are about 100 times larger than the electron-photon matrix elements,[21] but such enhancement factors are common for all the phonon modes. On the other hand, the values of exciton-phonon matrix elements are almost the same as the electron-phonon matrix elements.[21] Therefore, the exciton effects will not modify the relative intensity between the phonon modes. In Fig. 1(c),

8

we show an example of the calculation for intensity as a function of phonon frequency by including or excluding the modulation of optical interaction. The coherent phonon spectra shows both the RBM and LO peaks for a particular laser excitation energy of 1.15 eV. It can be seen that the LO intensity is enhanced significantly when taking the modulation of optical interaction into account (about 12 times larger than without considering the modulation of optical interaction), while the RBM intensity is just enhanced slightly (only by a factor of about 1.5).

To further understand the laser energy dependence of the spectra, we calculate the coherent phonon intensity for a given phonon frequency ω_m by considering different laser probe energy from 1.0-3.0 eV with an interval of 0.1 eV. In Fig. 2, we show absorption coefficients and coherent phonon spectra of the $(6,5)$ SWNT as a function of probe energy. For the coherent phonon spectra, we give the spectra both in the linear scale and logarithmic scale as shown in Figs. 2(b) and (c), respectively. The spectra are accompanied with the plot of absorption coefficient in Fig. 2(a) as a reference for showing the positions of the optical transition energy peaks. In Figs. 2(b) and (c), we compare the coherent G band phonon spectra (LO and iTO modes) with RBMs and also with oTO (out-of-plane TO) mode for the $(6,5)$ tube. In Fig. 2(b), we can see that the coherent RBM intensity and LO intensity are on the same order, with the RBM intensity being slighly larger than that of the LO intensity by a ratio of about 2.5 and 2.1 at E_{11} and E_{22}, respectively. These results indicate that modulations of optical matrix elements become important in enhancing the coherent G band intensity. It should be noted that the coherent iTO intensity is hundred times smaller than the LO intensity. Therefore, the coherent G band phonon spectra are mainly dominated by the LO phonon modes.

It is also interesting to see in Fig. 2(c) that there is a dip at 2 eV for the RBM phonons, which might be related with the zero value of the coherent RBM phonon amplitude.[14] The dip of RBM coherent phonon spectra could give information of photon energy that would correspond to the transition from expansion to contraction (or vice versa) of the SWNT diameter.[14] Moreover, we obtain two peaks at each transition energy for all phonon modes, consistent with some earlier works that reported the excitation energy dependence of coherent phonon intensity always shows a derivative-like behavior of the absorption coefficient.[4,11] The double-peak feature at each transition energy for the plots of coherent phonon intensity versus probe photon energy can be symmetric or asymmetric depending on whether or not
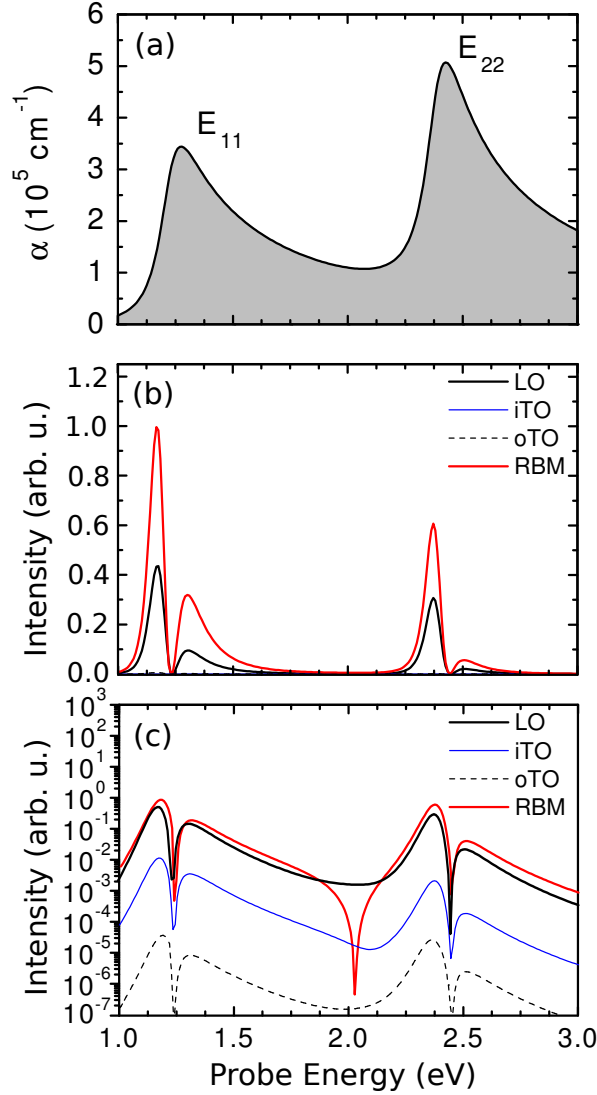
FIG. 2: (Color online) From top to bottom shows (a) absorption coefficient, (b) linearly scaled and (c) logarithmically scaled coherent phonon intensities as a function of probe energy for a (6,5) SWNT. The tube is photoexcited by a 1.15 eV Gaussian pump pulse linearly polarized along the tube axis (z axis) with a pulse width of $\tau_p = 10$ fs. The intensity is normalized to the maximum intensity of the RBM.

the excitonic effects are taken into account.[22] In this work, the double-peak lineshapes are asymmetric, i.e. the two peaks at each the transition energy do not have the same intensity, because we neglect the exciton effects for simplicty. It is also worth comparing the ratio of the coherent RBM and LO intensity obtained in this study with that in the experiment. For example, a pump-probe measurement by Lim *et al.* gave the RBM intensity of about
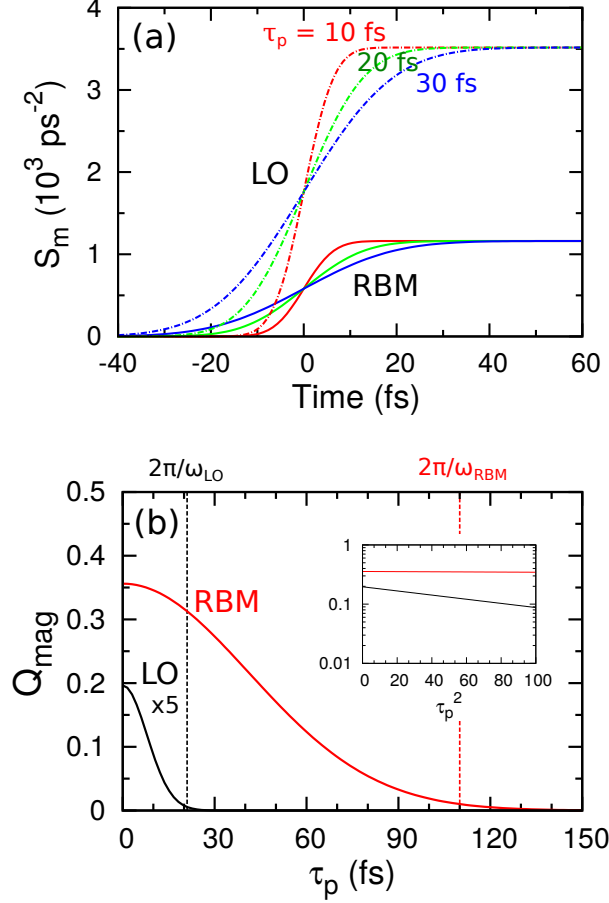
10

FIG. 3: (Color online) (a) Coherent phonon driving force (S_m) as a function of time for the RBM and LO phonon modes of the $(6,5)$ SWNT under E_{11} excitation. For each phonon mode in this plot, we consider three different values of pulse width (τ_p): 10 fs, 20 fs, and 30 fs. (b) Coherent phonon amplitude (Q_{mag}) for the RBM and LO phonon modes obtained analytically as a function of pulse width. Inset shows the logarithmic plot of the same amplitude as a function of squared pulse width.

eight times larger than the LO intensity.[9], thus the calculated relative intensity of RBM and LO is already on the same order-of-magnitude as obtained in the experiment. The small discrepancy, however, might come from the additional effect of the selection of laser pulse width τ_p.

B. Effects of laser pulse width

To discuss the effects of laser pulse width (τ_p) on the coherent phonon intensity, we can analytically model the driving function $S_m(t)$ of Eq. (2) by using the laser pulse in the form of Eq. (4) and then solve for $Q_m(t)$. By understanding the τ_p dependence of Q_m, we can qualitatively explain the trend of the coherent phonon intensity when τ_p is varied. As we can see from Eq. (2), $S_m(t)$ is proportional to the carrier density, $f_n(k,t)$, which can be obtained by integrating Eq. (3) with respect to time. For simplicity, we can write $S_m(t)$ to be directly proportional to the integration of $u(t)$,

$$S_m(t) \propto \int_{-\infty}^{t} A_p e^{-4t'^2 \ln 2/2\tau_p^2} dt'$$
$$\propto \frac{n_g F}{2c} \sqrt{\frac{\pi}{\ln 2}} \left[1 + \mathrm{erf}\left(\frac{2t \ln 2}{\tau_p} \right) \right], \tag{13}$$

where $\mathrm{erf}(x) = (2/\sqrt{\pi}) \int_0^x e^{-x'} dx'$ is the error function. To obtain the full equality between the left-hand and right-hand sides of Eq. (13), we can put an additional term of electron-phonon matrix element as also indicated in Eq. (2). This additional term along with the prefactor in the right-hand side of Eq. (13) form a constant A_m, which will change only when we have different phonon modes m. We can finally write the driving function as

$$S_m(t) = \frac{A_m}{2} \left[1 + \mathrm{erf}\left(\frac{2t \ln 2}{\tau_p} \right) \right]. \tag{14}$$

Next, to obtain a particular solution for $Q_m(t)$ from Eq. (1) with $S_m(t)$ in terms of Eq. (14), we can use a Fourier transform or Green's function method. In doing so, we assume that while there is a rise time in the carrier density that follows the integral of the envelope function for the pump pulse, for simplicity, we can approximate it by a Heaviside step function. This approximation should not affect the amplitude of the coherent phonon mode provided the pulse duration is short compared to the mode frequency. This allows us to write the equation for Q_m in terms of initial condition at $t = 0$. The corresponding solution for $Q_m(t)$ with an initial condition of $\dot{Q}_m(0) = 0$ (or equivalent to $Q_m(0)$ as a minimum value) is

$$Q_m(t) = \frac{A_m}{\omega_m^2} \left[1 - e^{-\omega_m^2 \tau_p^2/16 \ln 2} \cos(\omega_m t) \right]. \tag{15}$$

Having the solution of $Q_m(t)$, we can now discuss its dependence on τ_p. First, the value of A_m in Eqs. (14) and (15) can be obtained by fitting to the maximum value of the force

12

$S_m(t)$ simulated from the full microscopic treatment in Eq. (2). In Fig. 3(a), we show the simulated $S_m(t)$ for the RBM and LO mode of $(6,5)$ SWNT under E_{11} excitation with three different values of τ_p. We see that $S_m(t)$ for all cases show a step-like behavior with a width of τ_p, and thus consistent with Eq. (14). The maximum values of $S_m(t)$ only differ between different phonon modes. The fitted values of A_m for the RBM and LO mode are $1161.7\,\mathrm{ps}^{-2}$ and $3516.5\,\mathrm{ps}^{-2}$, respectively. In Fig. 3(b), we show the magnitude of Q_m, denoted as Q_{mag}, as a function of pulse width τ_p for the RBM and LO phonon modes. The definition for Q_{mag} is

$$Q_{\mathrm{mag}} = \frac{A_m}{\omega_m^2} e^{-\omega_m^2 \tau_p^2/16 \ln 2}, \tag{16}$$

which represents the difference between the maximum and minimum values of the coherent phonon oscillation amplitudes. We also have $2\pi/\omega_{\mathrm{RBM}} = 110\,\mathrm{fs}$ and $2\pi/\omega_{\mathrm{LO}} = 21\,\mathrm{fs}$ for the RBM and LO oscillation periods of the $(6,5)$ SWNT, respectively. We can see from Fig. 3(b) that as the pulse width increases, the coherent phonon amplitude quickly decays following the Gaussian shape of the spectrum of the laser pulse.[23] However, the rate of the amplitude decay depends on the phonon mode oscillation frequency or period, as clearly shown in the inset of Fig. 3(b). If the pulse width is much smaller than the phonon oscillation period, the amplitude will be enhanced. In this case, the LO phonon mode is enhanced more quickly than the RBM mode after the pulse width becomes shorter than the LO oscillation period. Therefore, as we have used $\tau_p = 10\,\mathrm{fs}$ in the simulation discussed earlier, the coherent LO intensity rapidly increases while at the same time the coherent RBM intensity increases more slowly. This could be the reason why we have a slightly different ratio of the RBM to the LO intensity since the coherent LO phonon amplitude is much more sensitive to the variation of the laser pulse width within the sub-10 fs region compared to the coherent RBM phonon amplitude.

IV. CONCLUSION

We have presented the mechanism by which a strong coherent G band signal could be generated in ultrafast pump-probe spectroscopy. Instead of the energy gap modulation mechanism which is dominant in the RBM case, we suggest that the modulations of electron-photon interaction as a function of time should be relevant to the coherent G band intensity. We also find an analytical formula that describes how a typical coherent phonon amplitude

behaves as a function of laser pulse width. The formula indicates that the G band (LO mode) intensity increases more rapidly than the RBM intensity by decreasing the pump laser pulse width, especially when the pulse is much shorter than each of the phonon mode period.

Acknowledgments

[1] R. Saito, G. Dresselhaus, and M. S. Dresselhaus, *Physical Properties of Carbon Nanotubes* (Imperial College Press, London, 1998).

[2] A. Jorio, M. S. Dresselhaus, and G. Dresselhaus, *Carbon Nanotubes: Advanced Topics in Synthesis, Structure, Properties, and Applications* (Springer-Verlag, Berlin, 2008).

[3] A. Gambetta, C. Manzoni, E. Menna, M. Meneghetti, G. Cerullo, G. Lanzani, S. Tretiak, A. Piryatinski, A. Saxena, R. L. Martin, and A. R. Bishop, Nat. Phys. **2**, 515–520 (2006).

[4] Y. S Lim, K. J. Yee, J. H. Kim, E. H. Haroz, J. Shaver, J. Kono, S. K. Doorn, R. H. Hauge, and R. E. Smalley, Nano Lett. **6**, 2696–2700 (2006).

[5] K. Kato, K. Ishioka, M. Kitajima, J. Tang, R. Saito, and H. Petek, Nano Lett. **8**, 3102–3108 (2008).

[6] J.-H. Kim, K.-J. Han, N.-J. Kim, K.-J. Yee, Y.-S. Lim, G. D. Sanders, C. J. Stanton, L. G. Booshehri, E. H. Hároz, and J. Kono, Phys. Rev. Lett. **102**, 037402 (2009).

[7] K. Makino, A. Hirano, K. Shiraki, Y. Maeda, and M. Hase, Phys. Rev. B **80**, 245428 (2009).

[8] J.-H. Kim, A. R. T. Nugraha, L. G. Booshehri, E. H. Haroz, K. Sato, G. D. Sanders, K.-J. Yee, Y.-S. Lim, C. J. Stanton, R. Saito, and J. Kono, Chem. Phys. **413**, 55–80 (2013).

[9] Y.-S. Lim, A. R. T. Nugraha, S.-J. Cho, M.-Y. Noh, E.-J. Yoon, H. Liu, J.-H. Kim, H. Telg, E. H. Haroz, G. D. Sanders, S.-H. Baik, H. Kataura, S. K. Doorn, C. J. Stanton, R. Saito, J. Kono, and T. Joo, Nano Lett. **14**, 1426–1432 (2014).

[10] H. J. Zeiger, J. Vidal, T. K. Cheng, E. P. Ippen, G. Dresselhaus, and M. S. Dresselhaus, Phys. Rev. B **45**, 768–778 (1992).

[11] J.-H. Kim, K.-J. Yee, Y.-S. Lim, L. G. Booshehri, E. H. Hároz, and J. Kono, Phys. Rev. B **86**, 161415 (2012).

[12] G. D. Sanders, C. J. Stanton, J.-H. Kim, K.-J. Yee, Y.-S. Lim, E. H. Hároz, L. G. Booshehri, J. Kono, and R. Saito, Phys. Rev. B **79**, 205434 (2009).

[13] A. Grüneis, R. Saito, Ge. G. Samsonidze, T. Kimura, M. A. Pimenta, A. Jorio, A. G. Souza Filho, G. Dresselhaus, and M. S. Dresselhaus, Phys. Rev. B **67**, 165402 (2003).

[14] A. R. T. Nugraha, G. D. Sanders, K. Sato, C. J. Stanton, M. S. Dresselhaus, and R. Saito, Phys. Rev. B **84**, 174302 (2011).

[15] Ge. G. Samsonidze, R. Saito, N. Kobayashi, A. Grüneis, J. Jiang, A. Jorio, S. G. Chou, G. Dresselhaus, and M. S. Dresselhaus, Appl. Phys. Lett. **85**, 5703 (2004).

[16] J. Jiang, R. Saito, Ge. G. Samsonidze, S. G. Chou, A. Jorio, G. Dresselhaus, and M. S. Dresselhaus, Phys. Rev. B **72**, 235408 (2005).

[17] S. L. Chuang, *Physics of optoelectronic devices* (Wiley, New York, 1995).

[18] V. N. Popov and L. Henrard, Phys. Rev. B **70**, 115407 (2004).

[19] A. Grüneis. *Resonance Raman spectroscopy of single wall carbon nanotubes.* PhD thesis, Tohoku University, Sendai, Japan, September 2004.

[20] A. R. T. Nugraha, R. Saito, K. Sato, P. T. Araujo, A. Jorio, and M. S. Dresselhaus, Appl. Phys. Lett. **97**, 091905 (2010).

[21] J. Jiang, R. Saito, K. Sato, J. S. Park, Ge. G. Samsonidze, A. Jorio, G. Dresselhaus, and M. S. Dresselhaus, Phys. Rev. B **75**, 035405 (2007).

[22] A. R. T. Nugraha, E. I. Rosenthal, E. H. Hasdeo, G. D. Sanders, C. J. Stanton, M. S. Dresselhaus, and R. Saito, Phys. Rev. B **88**, 075440 (2013).

[23] It is apparent that the coefficient in front of the cosine term in Eq. (15) is related to the Fourier transform of $u(t)$ given in Eq. (4). For a pulse shape in terms of Gaussian, the Fourier transform is also a Gaussian.